ELSEVIER

Contents lists available at ScienceDirect

# Chemical Engineering Journal

journal homepage: www.elsevier.com/locate/cej



# A metal organic framework-ultrafiltration hybrid system for removing selected pharmaceuticals and natural organic matter



Sewoon Kim<sup>a</sup>, Juan C. Muñoz-Senmache<sup>b</sup>, Byung-Moon Jun<sup>a</sup>, Chang Min Park<sup>c</sup>, Am Jang<sup>d</sup>, Miao Yu<sup>e</sup>, Arturo J. Hernández-Maldonado<sup>b</sup>, Yeomin Yoon<sup>a</sup>,\*

- <sup>a</sup> Department of Civil and Environmental Engineering, University of South Carolina, Columbia, 300 Main Street, SC 29208, USA
- Department of Chemical Engineering, University of Puerto Rico-Mayagüez Campus, Mayagüez, PR 00681, USA
- <sup>c</sup> Department of Environmental Engineering, Kyungpook National University, 80 Daehak-ro, Buk-gu, Daegu 41566, Republic of Korea
- d School of Civil and Architecture Engineering, Sungkyunkwan University, 2066 Seobu-ro, Jangan-16 Gu, Suwon, Gyeonggi-do 440-746, Republic of Korea
- <sup>e</sup> Department of Chemical and Biological Engineering, Rensselaer Polytechnic Institute, Troy, NY 12180, USA

#### HIGHLIGHTS

- A metal organic framework-ultrafiltration hybrid system was investigated for the removal of pharmaceuticals.
- MOF-UF system showed higher removal and low flux decline than PAC-UF system.
- The effect of natural organic matter on fouling was evaluated by using a resistance-in-series model.

#### ARTICLE INFO

#### Keywords: Ultrafiltration Metal-organic frameworks Pharmaceuticals Natural organic matter Fouling mechanism

#### ABSTRACT

In this study, we combined metal organic frameworks (MOFs) with ultrafiltration (UF) hybrid systems (MOF-UF) to treat selected pharmaceutically active compounds (PhACs), including ibuprofen and  $17\alpha$ -ethinyl estradiol, and natural organic matter (NOM) (humic acid and tannic acid; ratios of 10:0, 5:5, and 0:10). Due to the high tunable porosity of MOFs, these materials have strong potential for removing contaminants and reducing fouling in adsorbent-UF hybrid systems. The average retention rate of PhACs in MOF-UF (53.2%) was enhanced relative to the UF only (36.7%). The average retention rate of NOM in the MOF-UF (86.1%) was higher than that with UF only (75.7%). Also, the average normalized flux of NOM in the MOF-UF (0.79) was better than that with UF only (0.74). This is because the PhACs were effectively adsorbed on the MOF due to their strong porous characteristics. We compared MOF-UF and powdered activated carbon-UF (PAC-UF) systems in terms of retention rates and flux decline. The average retention rates for the MOF-UF were higher relative to PAC-UF, by 4.6% for PhACs and 6.9% for NOM. However, although the normalized flux in the MOF-UF was better than that in the PAC-UF, for both PhACs and NOM, severe flux decline for NOMs was seen for with the MOF-UF and PAC-UF. We evaluated the effects of NOM with respect to fouling by applying a resistance-in-series model and found that fouling was dominantly affected by the molecular sizes of the solutes in the solution.

#### 1. Introduction

In recent years, an increasing number of contaminants have been found in water resources due to climate change, population growth and rapid urbanization [1]. Particularly, various organic contaminants have generated widespread attention because of their potentially harmful impact on both the environment and humans. Pharmaceutically active compounds (PhACs) are one such emerging organic micropollutant, and have been increasingly detected in ground, surface, and wastewater due

to discharge and overuse of agricultural applications and according to more stringent standards for human health [2]. Although PhACs have been detected at low concentrations, they are potentially very hazardous for human health because they will return to aquatic environments, and then to the water supply, through the water cycle and exert physiologically adverse effects. Natural organic matter (NOM), which is composed of a heterogeneous structural mixture of aromatic and aliphatic compounds with varying molecular sizes, exists in virtually all environmental systems [3]. The presence of NOM not only

<sup>\*</sup> Corresponding author.

E-mail address: yoony@cec.sc.edu (Y. Yoon).

results in offensive odors and taste, but also acts as a potential precursor due to complexation with organic chemicals such as PhACs [4]. However, conventional water and wastewater treatment processes are not designed to completely degrade most PhACs and NOM [5,6]. As a result, these organic compounds can be excreted, and are thus continuously present in the environment. It is therefore necessary to study alternative water treatment systems to improve and enhance conventional technologies.

Among numerous modified processes, adsorption combined with ultrafiltration (UF) is one promising alternative water treatment system. Adsorption by porous materials is considered to be one of the most effective and simple processes for the removal of organic contaminants [7.8]. However, separating used porous materials remains a technological challenge [9]. UF is a low-pressure membrane process that has increasingly been applied to the removal of various organic pollutants and particles [10]. Occasionally, UF exhibits unsatisfactory performance, in terms of the removal of emerging organic pollutants, due to the limited retention ability of UF membranes [11]. Furthermore, membrane fouling is often caused by organic contaminants, especially NOM. UF with upstream adsorption has positive effects on performance in terms of the removal of organics, separating used adsorbents and reducing foulants such as NOM. Hence, many scientific studies have focused on UF hybrid systems coupled with adsorption [12]. However, to date, commercialized powdered activated carbon (PAC) has been used as an adsorbent in most hybrid systems (termed a 'PAC-UF' in this paper) and the study of alternative, superior adsorbents is still required to deal with emerging organic contaminants.

Metal organic frameworks (MOFs) are crystalline porous materials that consist of inorganic components, such as metal ion clusters, and organic components such as ligands. Due to their tunability and high porosity, the presence of coordinatively unsaturated sites, and varying pore architecture and composition, MOFs have an abundance of applications, for example in catalysis [13,14], separation [15,16], drug delivery [17,18], and gas storage [19,20]. Furthermore, recently, MOFs have been studied as potential adsorbents for eliminating various water pollutants, such as dyes [21,22], heavy metals [23,24], and organic contaminants [25,26]. Nevertheless, research on MOFs lacks diversity. For example, there have been no studies on hybrid MOF systems with UF (termed 'MOF-UF' in this paper). In particular, there have been no performance evaluations of the retention rates of micropollutants and NOM, or of the permeate flux in MOF-UF hybrid systems.

As the first attempt to address these issues, in this study we evaluated the removal of selected PhACs and NOM, using an MOF-UF hybrid system. The globally available pain killer, ibuprofen (IBP), and a common synthetic hormone, 17  $\alpha$ -ethinyl estradiol (EE2), were investigated in this study. Also, humic acid (HA) and tannic acid (TA) in three different ratios, and with different hydrophobicities and molecular sizes, were used as target NOMs. Two classical largely studied MOFs, namely iron-trimesic (MIL-100(Fe)) (where MIL stands for Material of Institute Lavoisier), and porous chromium-terephthalate (MIL-101(Cr)) were prepared in the laboratory and characterized using various analysis techniques [25]. Then, we carried out removal and filtration experiments for selected PhACs and NOM to evaluate the MOF-UF and compared the results to those obtained with a UF only, and with the PAC-UF. Finally, fouling mechanisms in the UF only, MOF-UF, and PAC-UF, were analyzed using a resistance-in-series model.

#### 2. Materials and methods

#### 2.1. PhACs/NOM and analytical methods

Two PhACs, IBP and EE2, were purchased from Sigma-Aldrich (St. Louis, MO, USA). Their detailed physicochemical properties are summarized in Table S1. The 10 mM stock solution of IBP and EE2, which were prepared in methanol, was placed in a separate beaker and diluted with deionized (DI) water to achieve an initial concentration of  $10 \, \mu M$ .

HA and TA were purchased from Sigma-Aldrich. Three different HA:TA ratios were used, all with total dissolved organic carbon concentrations (DOCs) of 10 mg/L. NOM 1, NOM 2, and NOM 3 correspond to 10:0, 5:5, 0:10 (HA:TA), respectively. In order to achieve the desired pH and background conductivity, each feed solution was adjusted by 1 M HCl or NaOH, and 0.1 M NaCl, respectively. Commercially available PAC (Evoqua Water Technologies, Pittsburgh, PA, USA) was used as a control group for the MOF.

The selected PhACs were collected into a 2 mL amber vial, and the concentrations of the compounds were measured by high-performance liquid chromatography with an ultraviolet (UV) detector (1200 Series; Agilent, Santa Clara, CA, USA). The single NOM (HA or TA) solutions were analyzed using a total organic carbon analyzer (Shimadzu, Kyoto, Japan) to determine the DOC concentration, and by an UV-visible (UV-Vis) spectrometer (DR-6000; Hach, Loveland, CO, USA). To obtain mixed NOM solutions, because HA is precipitated, whereas TA is stable under acidic conditions, we separated them by precipitation using a 5 M HCl at a pH value of 1.5. After the mixed sample had been separated over 24 h, we filtered it and then performed the DOC and UV-vis analyses.

#### 2.2. Synthesis of MIL-100(Fe) and MIL-101(Cr)

To prepare two MOFs in our laboratory, iron chips (99.98%), and trimesic acid (BTC, 95%) for MIL-100(Fe), and chrome(III) nitrate nonahydrate (Cr(NO<sub>3</sub>)<sub>3</sub>·9H<sub>2</sub>O, 99%), and terephthalic acid (TPA, 98%) for MIL-101(Cr), were purchased from Sigma-Aldrich. Nitric acid (HNO<sub>3</sub>, 60%), hydrofluoric acid (HF, 40%), and reagent alcohol (CH<sub>3</sub>CH<sub>2</sub>OH,  $\leq$  0.003%) were also obtained from Sigma-Aldrich.

MIL-100(Fe) [27] and MIL-101(Cr) [28] were synthesized by the solvothermal method following protocols reported in the literature with some modifications. Briefly, for the MIL-100(Fe), 1.0 Fe $^0$ :0.67 BTC:1.2 HNO $_3$ :2.0 HF:280 DI water was placed in a Teflon-lined steel autoclave. The autoclave was then placed in an electric oven at 150 °C for 12 h. After cooling, the solid orange products were recovered by filtration using a 10  $\mu m$  glass filter. The as-synthesized MIL-100(Fe) was purified in two steps using DI water at 90 °C for 3 h, and reagent alcohol at 65 °C for 5 h. After filtration, the purified MIL-100(Fe) was dried at 100 °C overnight and stored in a desiccator.

The reactant composition for the MIL-101(Cr) was 1.0 Cr  $(NO_3)_3$ :9 $H_2O:1.0$  TPA:1.0 HF:300 DI water, which was loaded in a Teflon-lined autoclave and placed in an electric oven at 210 °C for 8 h. After cooling to room temperature, the green-colored solids in the solution were filtered twice consecutively using 25 and 10  $\mu$ m glass filters. Then, to further purify the products, the as-synthesized MIL-101(Cr) was treated with reagent alcohol at 100 °C for 20 h, filtered off, and dried overnight at 100 °C. The purified MIL-101(Cr) was stored in a desiccator.

#### 2.3. Characterization

The structure of the MOFs was confirmed by X-ray diffraction (XRD) patterns, which were collected on an UTIMA III X-ray diffractometer (Rigaku, Tokyo, Japan) using Cu K $\alpha$  radiation ( $\lambda=1.5418$  Å) while operating at 40 kV and 44 mA. The Fourier transform-infrared (FT-IR) spectra were obtained using a Frontier spectrometer (PerkinElmer, Waltham, MA, USA), following the KBr pellet technique to detect the presence of functional groups. The morphology and element distribution of the MOFs was analyzed by transmission electron microscopy coupled with energy-dispersive spectroscopy (TEM-EDS) using a Titan G2 ChemiSTEM Cs Probe (FEI, Eindhoven, The Netherlands). X-ray photoelectron spectroscopy (XPS) measurements were carried out on a Quantera SXM (Physical Electronics, Inc., Chanhassen, MN, USA) with Al K $\alpha$  X-ray as the excitation source, to confirm the surface electronic states of the synthesized MOFs. Nitrogen adsorption and desorption equilibrium data were gathered at -196 °C using a Micromeritics ASAP

2020 static volumetric adsorption unit (Micromeritics Inc., Norcross, GA, USA). These data were used to estimate the materials textural properties. Prior to each analysis, MOFs were degassed at 150 °C under high vacuum for 12 h. Surface area was estimated using Brunauer-Emmett-Teller (BET) and Langmuir models. Pore diameter and pore volume were evaluated using the Barrett-Joyner-Halenda (BJH) method, and we obtained pore size distributions (PSDs) using Horvath-Kawazoe (H-K) and BJH analyses methods and to cover micropore and mesopore regions, respectively [29,30].

#### 2.4. Operation of the MOF-UF system

The UF only and MOF-UF performances were investigated using the selected PhACs and NOM removal and permeate flux decline were assessed by dead-end cell filtration (Sterlitech Co., Kent, WA, USA) with a 300 mL total feed volume. A UF membrane purchased from GE Osmonics Inc. (Minnetonka, MN, USA) was cut so that its active membrane surface area was 14.6 cm<sup>2</sup>. Based on the pure water permeability (PWP) test, only membranes with  $\leq 10\%$  permeability changes were used in this study. Both of the PhACs and NOM in three different ratios, were mixed with 20 mg/L of MOF for 2 h at 200 rpm for upstream adsorption. The adsorption conditions generally applied in water treatment plants (i.e., 5-50 mg/L with contact time of 1-5 h) were used [31,32]. The membrane system was operated at a transmembrane pressure of 520 kPa (75 psi) with stirring speed of 200 rpm. Permeate samples were collected every 20 mL until we obtained a permeate volume of 240 mL, corresponding to a volume concentration factor (VCF) in the range of 1.1-5 and water recovery of 7-80%. The VCF was evaluated using the following Eq. (1):

$$VCF = \frac{V_F}{V_R} = 1 + \frac{V_P}{V_R} \tag{1}$$

where  $V_F$  (mL),  $V_P$  (mL), and  $V_R$  (mL) are the initial feed, permeate, and retentate volumes, respectively.

#### 2.5. Determination of MOF-UF system performance

The membrane solute retention rate was calculated using the following Eq. (2):

Retention (%) = 
$$\left(1 - \frac{C_{p,VCF}}{C_{f,0}}\right) \times 100$$
 (2)

where  $C_{f,0}$  (mg/L) is the initial concentration in the feed, and  $C_{p,VCF}$  (mg/L) is the concentration in the permeate at the corresponding VCF. We also measured the permeate mass using an electronic balance (AV8101C; Ohaus, Pine Brook, NJ, USA) to determine the permeate flux decline, and quantified it using Eq. (3):

$$J = \frac{d_m}{\rho \cdot A_m \cdot d_t} \tag{3}$$

where J is the permeate flux (L/m²/h), m is the mass of permeate (kg),  $\rho$  is the density of permeate solution at 20 °C,  $A_m$  is the active membrane area (m²), and t is the sampling time (h). The obtained permeate fluxes were converted to normalized fluxes, which is the flux at the VCF divided by the corresponding initial flux; these fluxes were used to evaluate the membrane fouling of each system. Furthermore, a resistance-in-series model was used to predict the solute molecule transportation mechanisms in the UF-only and hybrid systems. In membrane filtration, Darcy's expression is commonly used to evaluate the permeate flux: [33,34]

$$J = \frac{\Delta P}{\eta(R_m + R_f)} = \frac{\Delta P}{\eta(R_m + R_{re} + R_{irr})} = \frac{\Delta P}{\eta(R_m + R_c + R_{ad})}$$
(4)

where  $\Delta P$  is the pressure drop across the membrane (kPa),  $\eta$  is the dynamic viscosity of the solvent (kg/m/s), and  $R_{\rm m}$  is the hydrodynamic

membrane resistance ( $m^{-1}$ ). The membrane fouling resistance ( $R_f$ ) is subdivided into reversible resistance ( $R_{re}$ ), and irreversible resistance ( $R_{irr}$ ), corresponding to the cake layer resistance ( $R_c$ ) and adsorptive fouling resistance ( $R_{ad}$ ), respectively. We used the previously defined equations to evaluate the proportions of these different resistance types.

#### 3. Results and discussion

#### 3.1. Characterization of MOFs

The synthesized MOFs were characterized by XRD, FT-IR, XPS, and TEM-EDS. The XRD patterns indicate that, by matching well with the simulated patterns, MIL-100(Fe) and MIL-101(Cr) were successfully synthesized under the applied conditions (Fig. S1a). Furthermore, the FT-IR spectrum of MIL-100(Fe) clearly exhibited peaks at 1635, 1383, 762, 711, and 485 cm<sup>-1</sup> (Fig. S1b), in excellent agreement with the corresponding functional groups of the known structure. [27,35] The peaks at 1635 and 1383 cm<sup>-1</sup> can be assigned to the carboxyl groups of organic ligands within MIL-100(Fe). The peaks of C-H bending are at 762 and 711 cm<sup>-1</sup>. Fe-O is indicated by the peak at 485 cm<sup>-1</sup>. The FT-IR spectrum of MIL-101(Cr) is similar to that obtained in previous studies (Fig. S1b) [28,36]. The vibrational stretching frequencies of O-C-O are at 1620 and 1400 cm<sup>-1</sup>, indicating the presence of dicarboxylate linkers within the MIL-101(Cr) structure. The peaks between 500 and 1600 cm<sup>-1</sup> can be assigned to the vibrations of benzene rings, including C=C at  $1510 \text{ cm}^{-1}$ , C-H at  $746 \text{ cm}^{-1}$ , -COO at  $587 \text{ cm}^{-1}$ . The XPS spectrum shows the surface chemical states of MIL-100(Fe) (Fig. S1c) and MIL-101(Cr) (Fig. S1d). For both MIL-100(Fe) and MIL-101(Cr), the XPS spectrum of C 1s contains two peaks at 284.8 and 288 eV, which correspond to phenyl and carboxyl signals, respectively [23,37]. The O 1 s peaks at 531.7 and 532 eV correspond to the Fe-O-C and Cr-O-C species in the XPS spectra of MIL-100(Fe) and MIL-101(Cr), respectively [38,39]. The Fe 2p spectrum for MIL-100(Fe) can be deconvoluted into two peaks centered at 712.3 and 724.8 eV, corresponding to the peaks of Fe 2p3/2 and Fe 2p1/2, respectively [40]. The spectrum of Cr 2p for MIL-101(Cr) was assigned to two peaks at 577 and 587 eV, corresponding to the Cr 2p3/2 and Cr 2p1/2 signals, respectively [37]. We evaluated the distributions of elements in MIL-100(Fe) and MIL-101(Cr) by carrying out EDS mapping analysis, and the results are shown in Fig. S1c and 1d (inset). The textural properties of both MOFs were estimated from N<sub>2</sub> adsorption-desorption isotherms gathered at 196 °C (77 K) (Table S2). Both MOFs exhibit large surface areas and pore volumes, as expected from highly microporous frameworks. Furthermore, a stack of PSD profiles for both MOFs materials shows the presence of pores with windows in the 9-12 Å region, as well as spherical cavities with sizes in the region 21-36 Å (Fig. S2). These values agree with data previously reported elsewhere [28,41]. Therefore, the XRD, FT-IR, XPS, TEM-EDS results and N2 isotherms lead to the conclusion that lab-made MIL-100(Fe) and MIL-101(Cr) was successfully synthesized and has strong potential for applications to adsorption-UF hybrid systems.

## 3.2. Performance of MOF-UF for PhACs

Fig. 1 shows the retention rate of selected PhACs by the UF only, MIL-100(Fe)-UF, and MIL-101(Cr)-UF as a function of VCF. The retention rates of IBP and EE2 for the UF only were 26.8–17.2% and 34.5–19.4% for pH 3, 49.4–40.5% and 34.3–25.1% for pH 7, and 44.1–38.6% and 65.3–46.3% for pH 11, respectively. In the case of the MOF-UF, the retention rates of IBP and EE2 were enhanced in comparison to the UF only. The retention rates of IBP/EE2 for the MIL-100(Fe)-UF were 40.8–23.8%/50.5–35.1%, 69.7–30.9%/47.1–39.1%, and 46.1–40.1%/61.6–52.9% for pH 3, 7, and 11, respectively. Furthermore, the retention rates of IBP/EE2 for the MIL-101(Cr)-UF were 54.9–24.0%/61.1–48.1%, 71.7–42.1%/60.5–45.1%, and 57.9–51.6%/72.2–66.1% for pH values of 3, 7 and 11, respectively. The retention

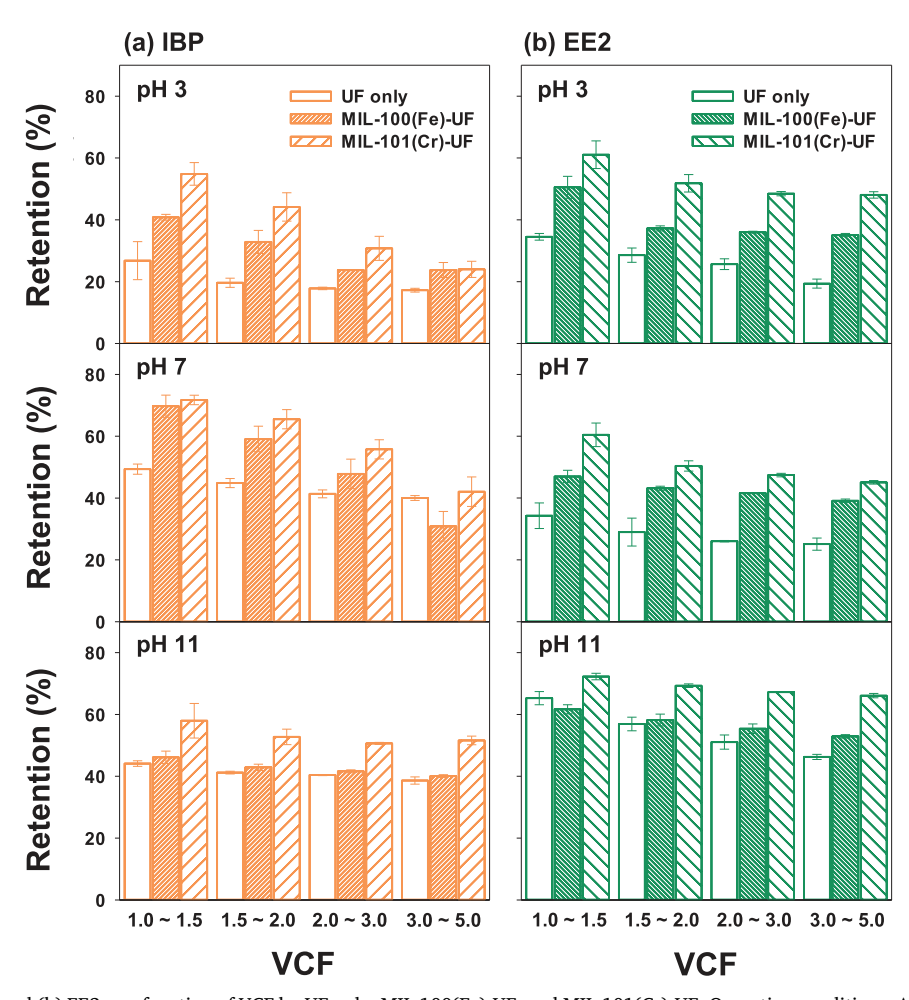


Fig. 1. Retention of (a) IBP and (b) EE2 as a function of VCF by UF only, MIL-100(Fe)-UF, and MIL-101(Cr)-UF. Operation conditions:  $\Delta P = 520$  kPa (75 psi); stirring speed = 200 rpm; MOF = 20 mg/L; initial selected PhAC concentration = 10  $\mu$ M; conductivity = 300  $\mu$ S/cm; pre-contact time with MOF = 2 h.

rate of three different systems is attributable to interaction associated with the physicochemical properties of membrane, MOFs, and selected PhACs. In this study, three different mechanisms govern the removal of those selected PhACs; which include size effect, electrostatic interactions, and hydrophobic interactions. Although the size exclusion effect is less apparent because the pore size of the membrane (26-30 Å as shown in Table S3) is bigger than the size of the PhACs (10.1 Å for IBP and 12.3 Å for EE2, as shown in Table S1), parts of the compound were removed according to the membrane size exclusion effect.[42,43] Furthermore, the contribution of MIL-101(Cr) to the retention rate was higher under all experimental conditions compared to the MIL-100(Fe). This is presumably because MIL-101(Cr) has a larger surface area and total pore volume as shown in Table S2, resulting in more adsorption. Furthermore, because the sizes of IBP (10.1 Å) and EE2 (12.3 Å) molecules are slightly larger than the pores of MIL-100(Fe), which act as windows (9 Å), IBP and EE2 molecules do not easily enter the pores of MIL-100(Fe) [41,44].

It is important to consider retention rate as a function of VCF so that appropriate technologies can be designed. Although the number of available vacant sites of the membrane and MOF for adsorption decreases as the VCF increases [25], the PhACs retention rate did not decrease significantly with increasing VCF in any of the three systems tested. Also, Fig. S3 shows that the normalized flux of the PhACs did not decrease significantly with increasing VCF. The membrane zeta potential, which enables us to assess the membrane surface charge density (Fig. S4a), suggests that the PhACs and MOF might not be significantly deposited or adsorbed on the membrane due to electrostatic repulsion [45]. Thus, we concluded that the retention rate and flux decline

associated with PhACs removal during filtration are somewhat slightly affected by the higher VCF of the MOF-UF.

To comprehensively investigate the retention mechanism, we plotted the retention performance by the proportions and  $\log D_{\rm OW}$  values (representing hydrophobicity) of the PhACs (Fig. 2). The retention rates of both PhACs were in the order: UF only < MIL-100(Fe)-UF < MIL-101(Cr)-UF. In particular, the retention of IBP (Fig. 2a) and EE2 (Fig. 2b) varied significantly as the pH increased above their pKa, exhibiting similar trends to their speciation curves. This can be explained in terms of charge exclusion, where dissociated PhACs are better retained [46]. Furthermore, EE2 exhibited slightly higher retention than IBP when they were present in similar proportions, due to its higher hydrophobicity (log  $D_{OW} = 3.9$  at pH 3 and 7, and 3.2 at pH 11, for EE2; and 3.8 at pH 3, 1.7 at pH 7, and 0.3 at pH 11 for IBP) [47]. It is noteworthy that the relative proportions and hydrophobicity of PhACs play an important role in the retention performance of MOF-UF. Fig. 2c and d shows the improvement in retention rate for the MOF-UF with variation in  $\log D_{\rm OW}$  relative to UF only. Due to their relatively higher hydrophobicity at lower pH values, the PhACs exhibited greater retention rate improvements due to hydrophobic attraction to the MOFs in the MOF-UF. In contrast, at higher pH values, PhACs with relatively lower hydrophobicity are less amenable to adsorption by the negatively charged MOF (estimated based on zeta potential; see Fig. S4b) and membrane. It is also interesting to note that the retention rates with the MIL-100(Fe)-UF and UF only were similar at pH 11; the retention (%) improvement is 1.6 for IBP and 1.5 for EE2. This could be explained by the fact that MIL-100(Fe) is decomposed at pH 11, changing to a

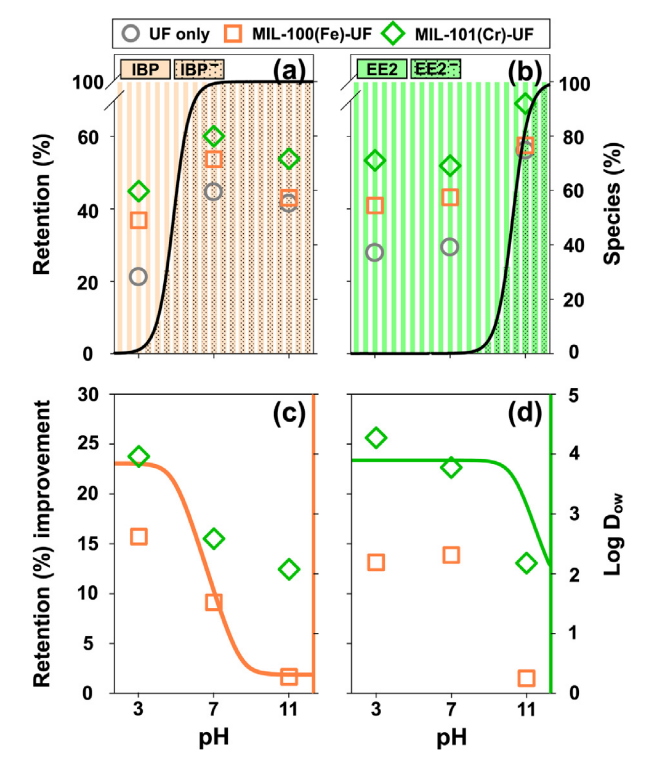


Fig. 2. Retention rate of (a) IBP, and (b) EE2 by UF only, MIL-100(Fe)-UF, and MIL-101(Cr)-UF at varying pH conditions with the fraction of species of IBP and EE2. Retention rate improvement of (c) IBP, and (d) EE2 by the hybrid system in comparison with the UF only system. Operation conditions:  $\Delta P=520\,kPa;$  stirring speed = 200 rpm; MOF = 20 mg/L; initial selected PhAC concentration =  $10\,\mu M;$  conductivity =  $300\,\mu S/cm;$  pre-contact time with MOF =  $2\,h.$ 

reddish-brown color [48,49]. Taken together, these observations indicate that the solution pH contributes considerably to the overall retention performance of the MOF-UF, in accordance with the physicochemical properties of the PhACs and stability of the MOF.

#### 3.3. Performance of MOF-UF for NOM

The retention rates of HA and TA under homogeneous and heterogeneous NOM conditions (HA:TA = 10:0 for NOM 1, 5:5 for NOM 2, and 0:10 for NOM 3) are presented in Fig. 3. NOM was removed at high rates by the MIL-100(Fe)-UF and MIL-101(Cr)-UF (74.2 and 78.8% for NOM 1, 86.8 and 88.0% for NOM 2, and 93.9 and 94.7% for NOM 3, respectively), while the UF only also showed reasonable retention rates (67.7% for NOM 1, 77.7% for NOM 2, and 81.7% for NOM 3). These data confirm the beneficial effects of MOF adsorption as an upstream treatment process. In particular, the highest retention rates for all NOM solutions were achieved with the MIL-101(Cr)-UF. As stated previously, these results accord with the textural properties of MOF. Also, the reason presumably is that greater  $\pi$ - $\pi$  interactions between NOM and MIL-101(Cr) provide slightly higher retention rates where, according to its chemical formula, MIL-101(Cr) has more aromatic rings than MIL-100(Fe) [50]. Moreover, because NOM, which contains negatively charged carboxy and phenolic hydroxyl groups, was in a dissociated state at pH 7 [51], the relatively positively charged MIL-101(Cr), as supported by the zeta potential analysis (Fig. S4b), resulted in electrostatic attraction to the NOM.

The results also indicated that the retention rate increased with the TA concentration. The TA stabilizes the particles in the solution more so than does HA due to its total potential energy, which incorporates both Brownian motion and van der Waals attraction [4,52]. Thus, TA can disrupt the aggregation of MOFs via electrostatic interaction and steric

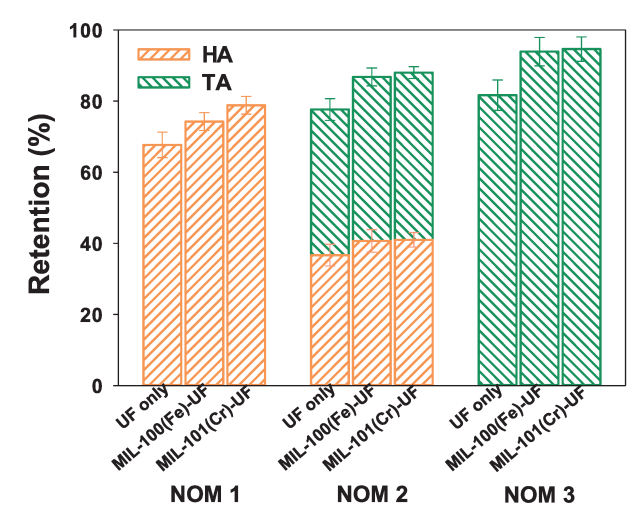


Fig. 3. Retention rate of the mixed HA and TA solutes by UF only, MIL-100(Fe)-UF, and MIL-101(Cr) for different NOM combinations. Operation conditions:  $\Delta P = 520 \, kPa; \quad stirring \quad speed = 200 \, rpm; \quad MOF = 20 \, mg/L; \quad initial NOM = 10 \, mg/L \ as \ DOC; \ pH = 7.0; \ conductivity = 300 \ \mu S/cm; \ pre-contact time with MOF = 2 h.$ 

repulsion, because more adsorption sites can be provided in the presence of TA solution. Furthermore, the molecular size distribution of TA ( $<17,000\,\mathrm{Da}$ ) is somewhat smaller than that of HA ( $170-22,600\,\mathrm{Da}$ ) [53,54]. Although HA is relatively hydrophobic compared to TA, HA can barely pass the MOF membrane pore due to its molecular size [55,56]. Furthermore, TA exhibited relatively larger declines in flux compared to HA (in the order NOM 1< NOM 2< NOM 3) (Fig. 4). Likewise, the relatively small TA molecules can be deposited on/in the membrane surface/pore more easily than HA, thus reducing the pore size and causing membrane fouling. These findings demonstrate that the MOF-UF performed better than the UF only, in terms of both the retention rate and flux decline of NOM. Also, TA can exacerbate permeate flux relative to HA due to the size of the TA molecules.

# ${\it 3.4.}$ Comparison between the MOF-UF and PAC-UF system: Retention and flux decline

The results of the previous experiment showed that the MIL-

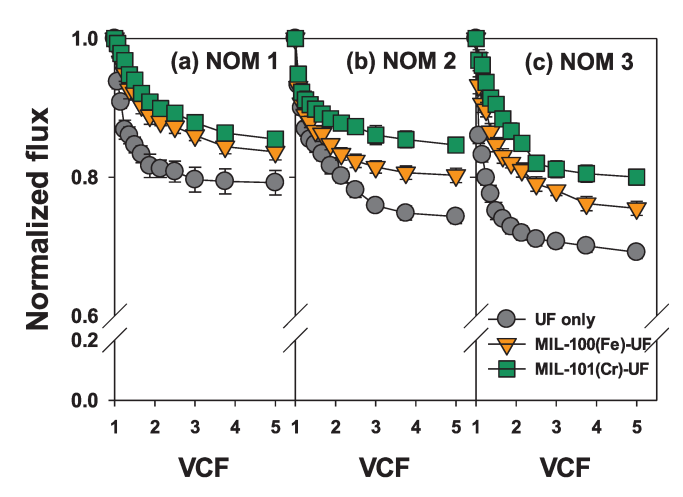


Fig. 4. Normalized Flux decline of (a) NOM 1, (b) NOM 2, and (c) NOM 3 for UF only, MIL-100(Fe)-UF, and MIL-101(Cr)-UF as a function of VCF. Operation conditions:  $\Delta P=520\,kPa;$  stirring speed = 200 rpm; MOF = 20 mg/L; initial NOM = 10 mg/L as DOC; pH = 7.0; conductivity = 300  $\,\mu\text{S/cm};$  pre-contact time with MOF = 2 h.

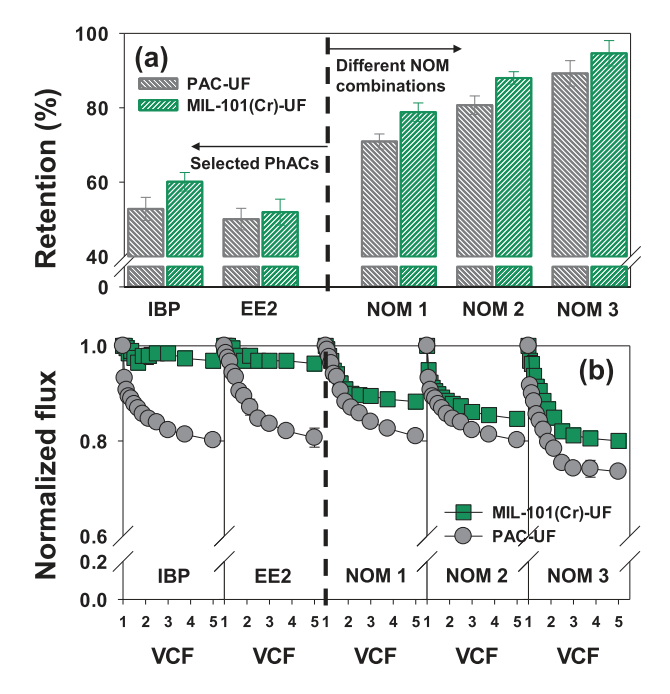


Fig. 5. (a) Retention rate and (b) normalized flux decline of selected PhACs and different NOM combinations by MIL-101(Cr)-UF and PAC-UF. Operation conditions:  $\Delta P = 520 \, kPa;$  stirring speed = 200 rpm; MOF = 20 mg/L; initial selected PhAC concentration = 10  $\mu M;$  initial NOM = 10 mg/L as DOC; pH = 7.0; conductivity = 300  $\mu S/cm;$  pre-contact time with MOF = 2 h.

101(Cr)-UF is most effective in terms of retention and permeate flux, for both PhACs and NOM. We carried out a performance comparison between the MOF-UF and PAC-UF (Fig. 5). The retention rates for the selected PhACs and NOM were slightly superior for the MIL-101(Cr)-UF compared to the PAC-UF at pH 7, by 7.3% for IBP, 1.9% for EE2, 7.9% for NOM 1, 7.3% for NOM 2, and 5.4% for NOM 3. This increased retention rate can be explained by the differences in textural characteristics between MIL-101(Cr) and PAC. Despite the similar pore diameters of the two adsorbents (26 Å for MIL-101(Cr), 21.9 Å for PAC), the greater total pore volume of MIL-101(Cr) (1.39 cm³/g) provides higher adsorption capability than PAC (0.24 cm³/g).

The normalized fluxes of IBP, EE2, NOM 1, NOM 2, and NOM 3, for the MIL-101(Cr)-UF at VCF 5, were 0.97, 0.96, 0.88, 0.85, and 0.80, respectively, compared to 0.83, 0.81, 0.81, 0.80, 0.74, respectively for the PAC-UF. As previously demonstrated (see Fig. S3), the MOF did not generate severe fouling with respect to PhACs. In contrast, use of PAC, which is more hydrophobic than MIL-101(Cr) [57,58], can result in marked fouling due to hydrophobic deposits on the polyamide membrane [59]. Thus, PAC-UF can cause a more serious decline in flux than the MIL-101(Cr)-UF for PhACs. In the case of NOM, despite the

normalized flux performance of the MIL-101(Cr)-UF being slightly better than that of the PAC-UF, both systems exhibited serious flux. As shown previously (see Fig. 4), this observation could be explained by the fact that NOM plays an important role in flux decline. Therefore, The MIL-101(Cr)-UF was superior to the PAC-UF with regard to retention and flux performance for both PhACs and NOM. However, the reasons for NOM fouling in the MOF-UF remain unclear, as do the reasons for the severe flux decline seen for the MOF-UF with respect to NOM.

#### 3.5. Fouling resistance in the MOF-UF

To evaluate the fouling characteristics and classify reversible/irreversible fouling in the hybrid systems, we assessed the UF only, MIL-101(Cr)-UF, and PAC-UF via a resistance-in-series model for three different NOM combinations that are all known to cause severe flux decline (Table 1). Both hybrid systems reduced total membrane fouling ( $R_t$ ), under all NOM combinations, relative to the UF only. Also, the  $R_t$  of the MIL-101(Cr)-UF was lower than that of PAC-UF. This is because the higher adsorption of NOM onto MIL-101(Cr) reduces the amount of fouling compared to PAC, leading to better  $R_t$  values. Furthermore, due to the relatively higher hydrophilicity of MIL-101(Cr), water can penetrate the membrane more easily relative to PAC [57,58]. The  $R_t$  value increased with increasing proportion of TA in the solution, consistent with the retention rate pattern shown in Fig. 5. With higher TA concentrations (although still smaller than the HA concentration), further blockage of the membrane surface and/or pores may occur [60,61].

The cake formation resistance ratio ( $R_{\rm c}/R_{\rm t}$ ) was in the order: NOM 3 < NOM 2 < NOM 1, while the adsorptive fouling resistance ratio ( $R_{\rm ad}/R_{\rm t}$ ) was in the order: NOM 1 < NOM 2 < NOM 3. This indicates that, while HA formed a cake layer on the membrane surface more readily than TA, TA was more easily adsorbed and/or blocked by the membrane pore, due to size exclusion effects. Moreover, a previous study reported that fouling by cake layers is considerable with large-sized solutes and fouling by adsorptive membranes is mainly affected by small-sized solutes during filtration [62,63].

Reversible and irreversible fouling is evaluated based on the  $\delta$  value, which is the total resistance per mass of retained NOM [63,64]. For the three different systems tested in this study, the  $\delta$  value increased with the TA concentration. Higher  $\delta$  values correspond to high potential for additional blockage and/or deposits on the membrane. Furthermore, the  $\delta$  values (×  $10^{12}$  m/g) of NOM 1 (88.7 for the MIL-101(Cr)-UF and 90.0 for the PAC-UF) and NOM 2 (99.1 for the MIL-101(Cr)-UF and 99.8 for the PAC-UF) were lower compared to the UF only (NOM 1, 95.8; NOM 2, 101). However, an increased value of  $\delta$  with the hybrid systems relative to the UF only was seen for NOM 3 (UF only, 95.8; MIL-101(Cr)-UF and PAC-UF, both 112). These results agree with the fact that the  $R_{\rm ad}$  values of NOM 1 and NOM 2 were significantly decreased by changing from the UF only to the hybrid systems, although the  $R_{\rm ad}$  value of NOM 3 decreased less markedly. Thus, the relatively small-sized NOM (TA in this study) could exacerbate irreversible fouling by

Table 1
Fouling resistances and cake layer characteristics as a function of unit retained DOC mass for different NOM combination by the different system according to resistance-in-series model.

	UF only			MIL-101(Cr)-UF			PAC-UF		
	NOM 1	NOM 2	NOM 3	NOM 1	NOM 2	NOM 3	NOM 1	NOM 2	NOM 3
$R_t (\times 10^{12} \mathrm{m}^{-1})$	94.5	98.4	106	83.0	87.3	94.9	84.8	91.3	99.6
$R_m (\times 10^{12} \mathrm{m}^{-1})$	73.4	73.1	73.3	73.3	73.2	73.3	73.5	73.2	73.2
$R_c (\times 10^{12} \mathrm{m}^{-1})$	15.9	12.4	11.1	10.2	6.63	6.00	13.4	7.92	7.50
$R_{ad} (\times 10^{12} \mathrm{m}^{-1})$	8.72	9.37	21.6	3.09	3.85	15.6	3.35	4.74	18.8
$R_c/R_t$	0.16	0.13	0.10	0.12	0.08	0.06	0.15	0.09	0.08
$R_{ad}/R_t$	0.09	0.10	0.20	0.04	0.04	0.16	0.04	0.05	0.19
$\delta (\times 10^{12} \mathrm{m/g})$	95.8	101	110	88.7	99.1	112	90.0	99.8	112

being adsorbed on the membrane pore. Consequently, resistance to both the cake layer and adsorptive membrane fouling were enhanced with use of the MIL-101(Cr). Also, the size exclusion effect, which causes irreversible fouling [63], was presumed to be the dominant reason for the decline in flux seen during NOM retention.

#### 4. Conclusions

In this study, we used MOF-UF hybrid systems to treat two PhACs (IBP and EE2) and NOM under three different ratios (HA:TA = 10:0, 5:5, and 0:10). Two classical MOFs were applied as upstream adsorbents: MIL-100(Fe) and MIL-101(Cr). For PhACs, the MOF-UF retention rate was better than that of the UF only under pH of 3, 7, and 11. Also, no severe fouling occurred in the case of the MOF-UF because the MOFs adsorbed the selected PhACs efficiently. In particular, MIL-101(Cr), with larger inner pores, exhibited higher solution stability than MIL-100(Fe), resulting in a higher PhAC retention rate. In the case of NOM, the retention rate and normalized flux with the MIL-101(Cr)-UF was better than that with the MIL-100(Fe)-UF and UF only. While increasing the TA concentration in the NOM solution resulted in a higher retention rate, the normalized flux in higher TA concentration solutions decreased significantly. As TA molecules are smaller than HA molecules, TA can readily adsorb onto/into the membrane surface/pore and MOF, resulting in higher retention and severe flux decline. Moreover, the MIL-101(Cr)-UF was superior to the PAC-UF in terms of both retention rate and permeate flux, for the selected PhACs and NOM. However, unlike PhACs, serious fouling was observed in NOM solutions, as previously stated. To evaluate the fouling mechanism, we applied a resistance-in-series model. The results showed that fouling is mainly in the form of cake layer fouling (reversible) for HA and adsorptive fouling (irreversible) for TA. These observations confirm that the performance of the MOF-UF hybrid system is superior to that of the UF only and PAC-UF, with respect to PhACs and NOM retention, and antifouling performance. Therefore, MOF-UF may be a suitable alternative technology to conventional system.

## Acknowledgements

This research was supported by the U.S. National Science Foundation (OIA-1632824). This work was also supported by the Korea Environment Industry & Technology Institute (KEITI) through Plant Research Program, funded by Korea Ministry of Environment (MOE) (88097).

### Appendix A. Supplementary data

Supplementary data to this article can be found online at https://doi.org/10.1016/j.cej.2019.122920.

#### References

- [1] S. Kim, C.M. Park, M. Jang, A. Son, N. Her, M. Yu, S. Snyder, D.-H. Kim, Y. Yoon, Aqueous removal of inorganic and organic contaminants by graphene-based nanoadsorbents: a review, Chemosphere 212 (2018) 1104–1124.
- [2] J. Wang, S. Wang, Activation of persulfate (PS) and peroxymonosulfate (PMS) and application for the degradation of emerging contaminants, Chem. Eng. J. 334 (2018) 1502–1517.
- [3] B.-M. Lee, Y.-S. Seo, J. Hur, Investigation of adsorptive fractionation of humic acid on graphene oxide using fluorescence EEM-PARAFAC, Water Res. 73 (2015) 242–251.
- [4] C. Jung, N. Phal, J. Oh, K.H. Chu, M. Jang, Y. Yoon, Removal of humic and tannic acids by adsorption-coagulation combined systems with activated biochar, J. Hazard. Mater. 300 (2015) 808–814.
- [5] L. Joseph, B.-M. Jun, M. Jang, C.M. Park, J.C. Muñoz-Senmache, A.J. Hernández-Maldonado, A. Heyden, M. Yu, Y. Yoon, Removal of contaminants of emerging concern by metal-organic framework nanoadsorbents: a review, Chem. Eng. J. 369 (2019) 928–946.
- [6] S. Kim, K.H. Chu, Y.A.J. Al-Hamadani, C.M. Park, M. Jang, D.-H. Kim, M. Yu, J. Heo, Y. Yoon, Removal of contaminants of emerging concern by membranes in water and wastewater: a review, Chem. Eng. J. 335 (2018) 896–914.

- [7] N. Jiang, R. Shang, S.G. Heijman, L.C. Rietveld, High-silica zeolites for adsorption of organic micro-pollutants in water treatment: a review, Water Res. 144 (2018) 145–161.
- [8] N.A. Khan, Z. Hasan, S.H. Jhung, Adsorptive removal of hazardous materials using metal-organic frameworks (MOFs): a review, J. Hazard. Mater. 244 (2013)
- [9] J. Löwenberg, A. Zenker, M. Baggenstos, G. Koch, C. Kazner, T. Wintgens, Comparison of two PAC/UF processes for the removal of micropollutants from wastewater treatment plant effluent: process performance and removal efficiency, Water Res. 56 (2014) 26–36.
- [10] S. Kim, D.W. Lee, J. Cho, Application of direct contact membrane distillation process to treat anaerobic digestate, J. Membr. Sci. 511 (2016) 20–28.
- [11] S. Kim, K.H. Chu, Y.A. Al-Hamadani, C.M. Park, M. Jang, D.-H. Kim, M. Yu, J. Heo, Y. Yoon, Removal of contaminants of emerging concern by membranes in water and wastewater: a review, Chem. Eng. J. 335 (2017) 896–914.
- [12] C. Stoquart, P. Servais, P.R. Bérubé, B. Barbeau, Hybrid membrane processes using activated carbon treatment for drinking water: a review, J. Membr. Sci. 411 (2012) 1–12.
- [13] L. Ma, J.M. Falkowski, C. Abney, W. Lin, A series of isoreticular chiral metal-organic frameworks as a tunable platform for asymmetric catalysis, Nature Chem. 2 (2010) 838.
- [14] Y.-B. Huang, J. Liang, X.-S. Wang, R. Cao, Multifunctional metal-organic framework catalysts: synergistic catalysis and tandem reactions, Chem. Soc. Rev. 46 (2017) 126–157.
- [15] J.S. Seo, D. Whang, H. Lee, S. Im Jun, J. Oh, Y.J. Jeon, K. Kim, A homochiral metal-organic porous material for enantioselective separation and catalysis, Nature 404 (2000) 982.
- [16] T. Rodenas, I. Luz, G. Prieto, B. Seoane, H. Miro, A. Corma, F. Kapteijn, F.X.L.I. Xamena, J. Gascon, Metal-organic framework nanosheets in polymer composite materials for gas separation, Nature Mater. 14 (2015) 48.
- [17] H. Zheng, Y. Zhang, L. Liu, W. Wan, P. Guo, A.M. Nyström, X. Zou, One-pot synthesis of metal-organic frameworks with encapsulated target molecules and their applications for controlled drug delivery, J. Am. Chem. Soc. 138 (2016) 962–968.
- [18] M.X. Wu, Y.W. Yang, Metal-organic framework (MOF)-based drug/cargo delivery and cancer therapy, Adv. Mater. 29 (2017) 1606134.
- [19] W. Xia, A. Mahmood, R. Zou, Q. Xu, Metal-organic frameworks and their derived nanostructures for electrochemical energy storage and conversion, Energy Environ. Sci. 8 (2015) 1837–1866.
- [20] D.K. Yoo, T.-U. Yoon, Y.-S. Bae, S.H. Jhung, Metal-organic framework MIL-101 loaded with polymethacrylamide with or without further reduction: effective and selective CO<sub>2</sub> adsorption with amino or amide functionality, Chem. Eng. J. 380 (2019) 122496.
- [21] E. Haque, J.E. Lee, I.T. Jang, Y.K. Hwang, J.-S. Chang, J. Jegal, S.H. Jhung, Adsorptive removal of methyl orange from aqueous solution with metal-organic frameworks, porous chromium-benzenedicarboxylates, J. Hazard. Mater. 181 (2010) 535–542.
- [22] H. Wang, X. Yuan, Y. Wu, G. Zeng, X. Chen, L. Leng, H. Li, Synthesis and applications of novel graphitic carbon nitride/metal-organic frameworks mesoporous photocatalyst for dyes removal, Appl. Catal. B 174 (2015) 445–454.
- [23] B.-J. Zhu, X.-Y. Yu, Y. Jia, F.-M. Peng, B. Sun, M.-Y. Zhang, T. Luo, J.-H. Liu, X.-J. Huang, Iron and 1, 3, 5-benzenetricarboxylic metal-organic coordination polymers prepared by solvothermal method and their application in efficient As(V) removal from aqueous solutions, J. Phys. Chem. C 116 (2012) 8601–8607.
- [24] F. Ke, L.-G. Qiu, Y.-P. Yuan, F.-M. Peng, X. Jiang, A.-J. Xie, Y.-H. Shen, J.-F. Zhu, Thiol-functionalization of metal-organic framework by a facile coordination-based postsynthetic strategy and enhanced removal of Hg2+ from water, J. Hazard. Mater. 196 (2011) 36–43.
- [25] Z. Hasan, J. Jeon, S.H. Jhung, Adsorptive removal of naproxen and clofibric acid from water using metal-organic frameworks, J. Hazard. Mater. 209 (2012) 151–157
- [26] Z. Hasan, N.A. Khan, S.H. Jhung, Adsorptive removal of diclofenac sodium from water with Zr-based metal-organic frameworks, Chem. Eng. J. 284 (2016) 1406–1413.
- [27] P. Horcajada, S. Surblé, C. Serre, D.-Y. Hong, Y.-K. Seo, J.-S. Chang, J.-M. Greneche, I. Margiolaki, G. Férey, Synthesis and catalytic properties of MIL-100 (Fe), an iron (III) carboxylate with large pores, Chem. Commun. 27 (2007) 2820–2822.
- [28] G. Férey, C. Mellot-Draznieks, C. Serre, F. Millange, J. Dutour, S. Surblé, I. Margiolaki, A chromium terephthalate-based solid with unusually large pore volumes and surface area, Science 309 (2005) 2040–2042.
- [29] S.U. Rege, R.T. Yang, Corrected Horváth-Kawazoe equations for pore-size distribution, AIChE J. 46 (2000) 734–750.
- [30] S. Lowell, J.E. Shields, M.A. Thomas, M. Thommes, Characterization of Porous Solids and Powders: Surface Area, Pore Size and Density, Springer Science & Business Media, 2012.
- [31] Y. Yoon, P. Westerhoff, S.A. Snyder, M. Esparza, HPLC-fluorescence detection and adsorption of bisphenol A,  $17\beta$ -estradiol, and  $17\alpha$ -ethynyl estradiol on powdered activated carbon, Water Res. 37 (2003) 3530–3537.
- [32] S. Kim, C.M. Park, A. Jang, M. Jang, A.J. Hernández-Maldonado, M. Yu, J. Heo, Y. Yoon, Removal of selected pharmaceuticals in an ultrafiltration-activated biochar hybrid system, J. Membr. Sci. 570 (2019) 77–84.
- [33] J. Mulder, Basic Principles of Membrane Technology, Springer Science & Business Media, 2012.
- [34] J.C. Crittenden, R.R. Trussell, D.W. Hand, K.J. Howe, G. Tchobanoglous, MWH's Water Treatment: Principles and Design, John Wiley & Sons, 2012.
- [35] P. Wang, H. Zhao, H. Sun, H. Yu, X. Quan, Porous metal-organic framework MIL-

- 100 (Fe) as an efficient catalyst for the selective catalytic reduction of  $NO_x$  with  $NH_3$ , RSC Adv. 4 (2014) 48912–48919.
- [36] Y. Hu, C. Song, J. Liao, Z. Huang, G. Li, Water stable metal-organic framework packed microcolumn for online sorptive extraction and direct analysis of naproxen and its metabolite from urine sample, J. Chromatogr. A 1294 (2013) 17–24.
- [37] M.-G. Jeong, D.H. Kim, S.-K. Lee, J.H. Lee, S.W. Han, E.J. Park, K.A. Cychosz, M. Thommes, Y.K. Hwang, J.-S. Chang, Decoration of the internal structure of mesoporous chromium terephthalate MIL-101 with NiO using atomic layer deposition, Microporous Mesoporous Mater. 221 (2016) 101–107.
- [38] R. Liang, S. Luo, F. Jing, L. Shen, N. Qin, L. Wu, A simple strategy for fabrication of Pd@ MIL-100 (Fe) nanocomposite as a visible-light-driven photocatalyst for the treatment of pharmaceuticals and personal care products (PPCPs), Appl. Catal. B 176 (2015) 240–248.
- [39] T.A. Vu, G.H. Le, C.D. Dao, L.Q. Dang, K.T. Nguyen, P.T. Dang, H.T. Tran, Q.T. Duong, T.V. Nguyen, G.D. Lee, Isomorphous substitution of Cr by Fe in MIL-101 framework and its application as a novel heterogeneous photo-Fenton catalyst for reactive dye degradation, RSC Adv. 4 (2014) 41185–41194.
- [40] F. Zhang, J. Shi, Y. Jin, Y. Fu, Y. Zhong, W. Zhu, Facile synthesis of MIL-100 (Fe) under HF-free conditions and its application in the acetalization of aldehydes with diols, Chem. Eng. J. 259 (2015) 183–190.
- [41] S.-H. Huo, X.-P. Yan, Metal-organic framework MIL-100 (Fe) for the adsorption of malachite green from aqueous solution, J. Mater. Chem. 22 (2012) 7449–7455.
- [42] K.J. Howe, M.M. Clark, Fouling of microfiltration and ultrafiltration membranes by natural waters, Environ. Sci. Technol. 36 (2002) 3571–3576.
- [43] K. Kim, A. Fane, R.B. Aim, M. Liu, G. Jonsson, I. Tessaro, A. Broek, D. Bargeman, A comparative study of techniques used for porous membrane characterization: pore characterization, J. Membr. Sci. 87 (1994) 35–46.
- [44] P. Horcajada, C. Serre, M. Vallet-Regí, M. Sebban, F. Taulelle, G. Férey, Metal-organic frameworks as efficient materials for drug delivery, Angew. Chemie 118 (2006) 6120–6124.
- [45] A.E. Childress, M. Elimelech, Relating nanofiltration membrane performance to membrane charge (electrokinetic) characteristics, Environ. Sci. Technol. 34 (2000) 3710–3716.
- [46] K.H. Chu, M. Fathizadeh, M. Yu, J.R. Flora, A. Jang, M. Jang, C.M. Park, S.S. Yoo, N. Her, Y. Yoon, Evaluation of removal mechanisms in a graphene oxide-coated ceramic ultrafiltration membrane for retention of natural organic matter, pharmaceuticals, and inorganic salts, ACS Appl. Mater. Inter. 9 (2017) 40369–40377.
- [47] C. Jung, J. Park, K.H. Lim, S. Park, J. Heo, N. Her, J. Oh, S. Yun, Y. Yoon, Adsorption of selected endocrine disrupting compounds and pharmaceuticals on activated biochars, J. Hazard. Mater. 263 (2013) 702–710.
- [48] Y. Xu, L. Xu, S. Qi, Y. Dong, Z.U. Rahman, H. Chen, X. Chen, In situ synthesis of MIL-100 (Fe) in the capillary column for capillary electrochromatographic separation of small organic molecules, Anal. Chem. 85 (2013) 11369–11375.
- [49] I. Bezverkhyy, G. Weber, J.-P. Bellat, Degradation of fluoride-free MIL-100 (Fe) and MIL-53 (Fe) in water: effect of temperature and pH, Microporous Mesoporous Mater. 219 (2016) 117–124.
- [50] H. Hyung, J.-H. Kim, Natural organic matter (NOM) adsorption to multi-walled

- carbon nanotubes: effect of NOM characteristics and water quality parameters, Environ. Sci. Technol. 42 (2008) 4416–4421.
- [51] C. Sun, B. Xiong, Y. Pan, H. Cui, Adsorption removal of tannic acid from aqueous solution by polyaniline: analysis of operating parameters and mechanism, J. Colloid. Interf. Sci. 487 (2017) 175–181.
- [52] T. Phenrat, J.E. Song, C.M. Cisneros, D.P. Schoenfelder, R.D. Tilton, G.V. Lowry, Estimating attachment of nano-and submicrometer-particles coated with organic macromolecules in porous media: development of an empirical model, Environ. Sci. Technol. 44 (2010) 4531-4538.
- [53] D. Lin, B. Xing, Tannic acid adsorption and its role for stabilizing carbon nanotube suspensions, Environ. Sci. Technol. 42 (2008) 5917–5923.
- [54] C.-F. Lin, Y.-J. Huang, O.J. Hao, Ultrafiltration processes for removing humic substances: effect of molecular weight fractions and PAC treatment, Water Res. 33 (1999) 1252–1264.
- [55] R. Beckett, Z. Jue, J.C. Giddings, Determination of molecular weight distributions of fulvic and humic acids using flow field-flow fractionation, Environ. Sci. Technol. 21 (1987) 289–295.
- [56] Y.-P. Chin, G. Aiken, E. O'Loughlin, Molecular weight, polydispersity, and spectroscopic properties of aquatic humic substances, Environ. Sci. Technol. 28 (1994) 1853–1858.
- [57] F. Zhang, X. Sang, X. Tan, C. Liu, J. Zhang, T. Luo, L. Liu, B. Han, G. Yang, B.P. Binks, Converting metal-organic framework particles from hydrophilic to hydrophobic by an interfacial assembling route, Langmuir 33 (2017) 12427–12433.
- [58] B.N. Bhadra, K.H. Cho, N.A. Khan, D.-Y. Hong, S.H. Jhung, Liquid-phase adsorption of aromatics over a metal-organic framework and activated carbon: effects of hydrophobicity/hydrophilicity of adsorbents and solvent polarity, J. Phys. Chem. C 119 (2015) 26620–26627.
- [59] F.O. Perreault, M.E. Tousley, M. Elimelech, Thin-film composite polyamide membranes functionalized with biocidal graphene oxide nanosheets, Environ. Sci. Technol. Letters 1 (2013) 71–76.
- [60] K.H. Chu, V. Shankar, C.M. Park, J. Sohn, A. Jang, Y. Yoon, Evaluation of fouling mechanisms for humic acid molecules in an activated biochar-ultrafiltration hybrid system, Chem. Eng. J. 326 (2017) 240–248.
- [61] G. Huang, F. Meng, X. Zheng, Y. Wang, Z. Wang, H. Liu, M. Jekel, Biodegradation behavior of natural organic matter (NOM) in a biological aerated filter (BAF) as a pretreatment for ultrafiltration (UF) of river water, Appl. Microbiol. Biotechnol. 90 (2011) 1795–1803.
- [62] A. Zularisam, A. Ismail, R. Salim, Behaviours of natural organic matter in membrane filtration for surface water treatment—a review, Desalination 194 (2006) 211–231.
- [63] K.H. Chu, Y. Huang, M. Yu, N. Her, J.R. Flora, C.M. Park, S. Kim, J. Cho, Y. Yoon, Evaluation of humic acid and tannic acid fouling in graphene oxide-coated ultrafiltration membranes, ACS Appl. Mater. Inter. 8 (2016) 22270–22279.
- [64] H. Susanto, M. Ulbricht, High-performance thin-layer hydrogel composite membranes for ultrafiltration of natural organic matter, Water Res. 42 (2008) 2827–2835.